Available online at www.sciencedirect.com

ScienceDirect

IFAC PapersOnLine 54-3 (2021) 281–286

Mixing strategies combined with shape design to enhance productivity of a raceway pond

Olivier Bernard * **Liu-Di Lu** *,** **Julien Salomon** **

* *Université Nice Côte d'Azur, INRIA Sophia Antipolis Méditerranée, BIOCORE Project-Team, BP93, 06902 Sophia-Antipolis Cedex, France (e-mail: olivier.bernard@inria.fr)*

** *INRIA Paris, ANGE Project-Team, 75589 Paris Cedex 12, France and Sorbonne Université, CNRS, Laboratoire Jacques-Louis Lions, 75005 Paris, France (e-mail: liudi.lu@inria.fr, julien.salomon@inria.fr)*

Abstract: This paper focuses on mixing strategies and designing shape of the bottom topographies to enhance the growth of the microalgae in raceway ponds. A physical-biological coupled model is used to describe the growth of the algae. A simple model of a mixing device such as a paddle wheel is also considered. The complete process model was then included in an optimization problem associated with the maximization of the biomass production. The results show that non-trivial topographies can be coupled with some specific mixing strategies to improve the microalgal productivity.

Keywords: Industrial biotechnology, Parametric optimization, Discrete optimization, Hydrodynamics, Han model, Microalgal raceway

1. INTRODUCTION

Microalgae are photosynthetic organisms whose potential has been proven in the last decade for several biotechnological applications (e.g. Chisti, 2007). They can be cultivated industrially for cosmetics, pharmaceuticals, food complements and green energy applications (Wijffels and Barbosa, 2010). These micro-organisms can be massively cultivated in closed (e.g. Perner et al., 2003) or open photobioreactors. According to the applications, the light can be artificial (for high added value products) or natural.

In this paper, we focus on the cultivation of the algae in a raceway pond. The water is mixed and set in motion in this circular basin by means of a paddle wheel (Chiaramonti et al., 2013). Studies have shown that the topographies can have an impact on the growth rate of the algae (Bernard et al., 2021a), whereas mixing the microalgae guarantees that each cell have regularly access to light and necessary nutrients to growth (Demory et al., 2018). In this paper, we extend the study of Bernard et al. (2021a) by investigating the optimal combinations between mixing strategies and bottom topographies to enhance algal productivity. We show that non trivial topographies can be obtained associated with some specific mixing strategies.

The paper is organized as follows. In Section 2, we describe the hydrodynamical, the biological and the mixing models and we define the coupled model. Afterwards, we present the optimization problem together with numerical optimization procedure in two frameworks. Eventually, we show some numerical tests to illustrate our approach and study the influence of the topography, depth of the raceway and mixing strategy in the optimization process.

2. RACEWAY MODELING

The raceway system can be described by a coupling between the hydrodynamics and the dynamics of the photosystems in the algae. The raceway is set in motion by a paddle wheel mixing the algae and modifying their depth and therefore the light flux that they see.

2.1 Shallow water equations

We model the hydrodynamics of our system by the shallow water equations, which is derived from the free surface incompressible Navier-Stokes equations (see for instance Gerbeau and Perthame. (2001)). More precisely, we consider the smooth steady state solutions of the shallow water equations in a laminar regime, which are governed by the following partial differential equations:

$$\partial_x(hu) = 0, \quad \partial_x(hu^2 + g\frac{h^2}{2}) = -gh\partial_x z_b,$$

where h stands for the water elevation, u represents the horizontal averaged velocity of the water, the constant g is the gravitational acceleration, and z_b defines the topography. The free surface η is defined by $\eta := h + z_b$ and the averaged discharge $Q = hu$. A schematic representation of this system is given in Fig. 1.

The z axis represents the vertical direction and the x axis represents the horizontal direction. Besides, L stands for the length of one lap of the raceway pond and I_s

10.1016/j.ifacol.2021.08.255

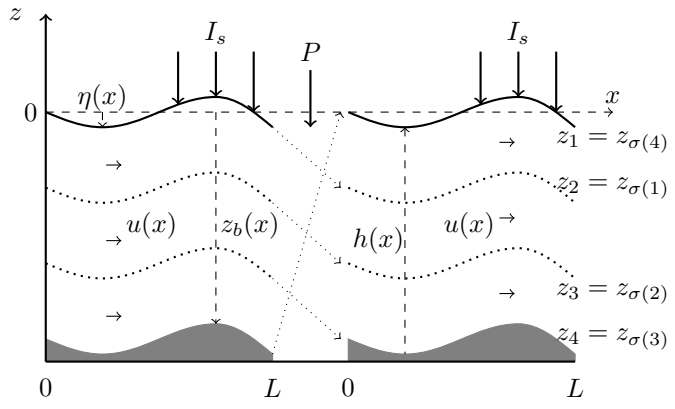

Fig. 1. Representation of the hydrodynamic model with an example of mixing device (P). Here, P corresponds to the cyclic permutation $\sigma = (1\ 2\ 3\ 4)$.

represents the light intensity at the free surface (assumed to be constant).

The Froude number for the steady state is defined by $Fr = u/\sqrt{gh}$. The situation $Fr < 1$ corresponds to the subcritical case (i.e. the flow regime is fluvial) while $Fr > 1$ is to the supercritical case (i.e. the flow regime is torrential). In the following studies, we limit ourselves to the subcritical case. Following the procedure from Bernard et al. (2021a), the topography can be computed solved by:

$$z_b = \frac{M_0}{g} - \frac{Q_0^2}{2gh^2} - h, \tag{1}$$

where Q_0 and M_0 are two positive constants.

2.2 Lagrangian trajectories and light intensity

Incompressibility and a kinematic condition at bottom can then be used to obtain the following equation of the Lagrangian trajectory of the algae (Equation (12)-(15) Bernard et al., 2021a).

$$z(x) = \eta(x) + \frac{h(x)}{h(0)}(z(0) - \eta(0)), \tag{2}$$

where $z(0)$ is the initial position of the algae.

To obtain the light intensity I at depth z, we use the Beer-Lambert law to describe the light attenuation:

$$I(x, z) := I_s \exp\big(-\varepsilon(\eta(x) - z)\big), \tag{3}$$

where ε is the extinction coefficient. Using (2) in (3), we find the light intensity captured by the algae following the trajectories $z(x)$ in one lap of the raceway

$$I(x, z) = I_s \exp\big(-\varepsilon\frac{h(x)}{h(0)}(\eta(0) - z(0))\big).$$

Given initial conditions $h(0), z_b(0)$, then $\eta(0) = h(0) + z_b(0)$, we see that computing I on a trajectory only requires to know the initial position $z(0)$ and the water elevation $h(x)$ which is obtained by solving (1).

2.3 Han model

The dynamics of the light harvesting complexes in the chloroplasts is controlled by the amount of light perceived by the algal cells. They can be described by the Han model (Han., 2001), in which the reaction centers are assumed to have three different states: open and ready to harvest a photon (A), closed while processing the absorbed photon energy (B), or inhibited if several photons have been absorbed simultaneously leading to an excess of energy (C). The evolution of the state A, B, C satisfies the following dynamical system

$$\begin{cases} \dfrac{\mathrm{d}A}{\mathrm{d}t} = -\sigma I A + \frac{B}{\tau}, \\ \dfrac{\mathrm{d}B}{\mathrm{d}t} = \sigma I A - \frac{B}{\tau} + k_r C - k_d \sigma I B, \\ \dfrac{\mathrm{d}C}{\mathrm{d}t} = -k_r C + k_d \sigma I B, \end{cases}$$

where A, B, C are the relative frequencies of the three possible states which satisfy $A+B+C = 1$, the coefficients σ, τ, k_r and k_d represent the specific photon absorption, the turnover rate, the photosystem repair rate and the damage rate, respectively. As shown in Lamare et al. (2019), one can use a fast-slow approximation and singular perturbation theory to reduce this system to a single evolution equation:

$$\frac{\mathrm{d}C}{\mathrm{d}t} = -\alpha(I)C + \beta(I), \tag{4}$$

where $\beta(I) = k_d\tau\frac{(\sigma I)^2}{\tau\sigma I+1}$ and $\alpha(I) = \beta(I) + k_r$. Then following Bernard et al. (2021a), we obtain a time-free reformulation of (4), namely

$$\frac{\mathrm{d}C}{\mathrm{d}x} = \big(-\alpha(I)C + \beta(I)\big)\frac{h}{Q_0}, \tag{5}$$

where all the functions on the right-hand side only depend on x. The net specific growth rate is then obtained by balancing photosynthesis and respiration, which gives

$$\mu(C, I) := \gamma(I)C + \zeta(I), \tag{6}$$

where $\gamma(I) = \frac{k\sigma I}{\tau\sigma I+1}$ and $\zeta(I) = \gamma(I) - R$. Here k stands for a factor that links received energy and growth rate. The term R represents the respiration rate. The average net specific growth rate over the domain is then defined from (6) by

$$\bar{\mu} := \frac{1}{V}\int_0^L \int_{z_b}^{\eta} \mu\big(C(x,z), I(x,z)\big)\mathrm{d}z\mathrm{d}x. \tag{7}$$

This will be the principle function of our following studies.

Remark 1. The dynamic of the biomass concentration is derived from (6): $\dfrac{\mathrm{d}X}{\mathrm{d}t} = \bar{\mu}X - DX$, where D is the dilution rate. The extinction coefficient ε depends on X as follows. The system is perfectly mixed, then the concentration is homogeneous so ε is a constant independent of space. In general, the extinction coefficient ε is an affine function of the biomass X (see Martínez et al. (2018))

$$\varepsilon(X) = \alpha_0 X + \alpha_1, \tag{8}$$

where $\alpha_0 > 0$ stands for the specific light extinction coefficient of the microalgae specie and α_1 defines the background turbidity that summarizes the light absorption and diffusion due to all non-microalgae components.

We assume that the algal biomass X in the raceway is controlled at a concentration which meets the so-called compensation condition (see Masci et al. (2010); Grognard et al. (2014)). This condition means that photosynthesis equilibrates respiration in the darkest layer of the raceway. In other terms, at steady-state, the growth rate μ at the (average) bottom depth $\bar{z}_b$ is 0, i.e., $-\gamma(I_{\bar{z}_b})\frac{\beta(I_{\bar{z}_b})}{\alpha(I_{\bar{z}_b})} +$

$\zeta(I_{\bar{z}_b}) = 0$. Solving the above equation provides a value of $I_{\bar{z}_b}$ thus of the extinction coefficient $\varepsilon(X)$, and finally of the biomass concentration X. In the sequel we assume that an appropriate control strategy maintains the biomass around this value by playing on the dilution rate D.

2.4 Vertical discretization of the system

In order to compute numerically (7), let us consider a uniform vertical discretization of the initial position $z(0)$ for N_z cells: $z_n(0) = \eta(0) - \frac{n-\frac{1}{2}}{N_z}h(0), n = 1, \dots, N_z$. From (2), we obtain $z_n(x) - z_{n+1}(x) = \frac{1}{N_z}h(x), n = 1, \dots, N_z$, meaning that the cell distribution remains uniform along the trajectories. To simplify notations, we write $I_n(x)$ instead of $I(x, z_n)$ hereafter.

Let $C_n(x)$ (resp. $I_n(x)$) the photo-inhibition state (resp. the light intensity) associated with the trajectories $z_n(x)$. Then the semi-discrete average net specific growth rate of (7) can be defined by

$$\bar{\mu}_\Delta := \frac{1}{VN_z}\sum_{n=1}^{N_z}\int_0^L \mu(C_n(x), I_n(x))h(x)\mathrm{d}x. \tag{9}$$

2.5 Paddle wheel modeling

Recent studies have shown that the paddle wheel played a key role in a raceway ponds system Chiaramonti et al. (2013); Demory et al. (2018), where the paddle wheel set this hydrodynamic-biologic coupling system in motion. At the same time, it modifies the elevation of the algae passing through it, and thus giving successively access to light to all the population. This mixing device has been studied in Bernard et al. (2021b), where a flat topography has been considered and the mixing procedure is assumed to be perfect, meaning that at each new lap, the algae at depth $z_n(0)$ are entirely transferred into the position $z_{\sigma(n)}(0)$ when passing through the mixing device. In the current study, we still assume that we can design a mixing setup achieving an ideal rearrangement of trajectories, and we consider the case when the topography is no longer flat.

We denote by $\mathcal{P}$ the set of permutation matrices of size $N_z \times N_z$ and by $\mathfrak{S}_{N_z}$ the associated set of permutations of N_z elements. This model is depicted schematically on an example in Fig. 1.

2.6 Periodic regime

Recall that L is the length of one lap of the raceway pond. We assume that the state C is KL-periodic in the sense that after K times of passing the device (P), $C^K(0) = C(0)$. A natural choice for K is the order of the permutation P.

Following arguments similar to that in (Proposition 1, Lemma 1 Bernard et al., 2021b), it can be proved that if the system is KL-periodic, then it is L-periodic. Hence, the average growth rate $\bar{\mu}$ for K laps equals to the average growth rate $\bar{\mu}$ for a single lap. This will help us in simplifying the formulation of the optimization problem considered in the next section. In addition, the computations to solve the optimization problem will be reduced, since the CPU time required to assess the productivity gain of a permutation will not depend on its order.

Remark 2. In the setting presented in Bernard et al. (2021b), when the system is assumed to be periodic $C(0)$, hence C depends on the permutation matrix P. In the current study, the state C will also depend on the permutation matrix P that we denote C^P hereafter.

3. OPTIMIZATION

In this section, we define the optimization problem associated with our biological-hydrodynamical-permutation model. As mentioned in Section 2.1, a given smooth topography z_b corresponds to a unique water elevation h under the assumption that flow remains in a subcritical regime. On the other hand, since we consider a 1D framework, the volume of our system is simply given by $V = \int_0^L h(x)\mathrm{d}x$. Since this quantity plays an important role in raceway design, and need to be easily handled. Therefore, we choose to parameterize the water elevation h. Given an optimal parameter a^*, the associated optimal topography can be determined by means of (1). An example of parameterization consists in writing h as a truncated Fourier series

$$h(x, a) = a_0 + \sum_{m=1}^{M} a_m \sin(2m\pi\frac{x}{L}), \tag{10}$$

such parameterization allows us to control the volume since $V = a_0 L$.

For simplicity of notation, we omit x in the notation and rather denote explicitly that the functions depend on a.

3.1 Optimization problem for constant reactor volume

In this section, we assume that the volume of the reactor is constant. Such situation can be obtained, e.g., by using the parameterization (10) with a fixed a_0. Consider then a vector $a := [a_1, \cdots, a_M] \in \mathcal{R}^M$, which will be the variable to be optimized. The objective function is then defined from (9) by

$$\bar{\mu}_\Delta^P(a) = \frac{1}{VN_z}\sum_{n=1}^{N_z}\int_0^L \mu(C_n^P, I_n(a))h(a)\mathrm{d}x, \tag{11}$$

where C_n^P satisfies the following parameterized version of (5) with a periodic condition

$$\begin{cases} \dfrac{\mathrm{d}C_n^P}{\mathrm{d}x} &= \big(-\alpha(I(a))C + \beta(I(a))\big)\frac{h(a)}{Q_0}, \\ PC_n^P(L) &= C_n^P(0). \end{cases} \tag{12}$$

Our optimization problem then reads:

Find a permutation matrix $P_{\max}$ and a parameter vector a^* solving the maximization problem:

$$\max_{P\in\mathcal{P}}\max_{a\in\mathcal{R}^M}\bar{\mu}_\Delta^P(a).$$

3.2 Optimization procedure for constant reactor volume

For a given permutation matrix $P \in \mathcal{P}$, the Lagrangian of (11) can then be written by

$$\begin{aligned}&\mathcal{L}^P(C, p, a)\\ &= \frac{1}{VN_z}\sum_{n=1}^{N_z}\int_0^L \big(-\gamma(I_n(a))C_n^P + \zeta(I_n(a))\big)h(a)\mathrm{d}x\\ &- \sum_{n=1}^{N_z}\int_0^L p_n^P\Big(\frac{\mathrm{d}C_n^P}{\mathrm{d}x} + \big(\alpha(I_n(a))C_n^P - \beta(I_n(a))\big)\frac{h(a)}{Q_0}\Big)\mathrm{d}x,\end{aligned}$$

where p_n^P is the Lagrange multiplier associated with the constraint (12).

The optimality system is obtained by cancelling all the partial derivatives of $\mathcal{L}^P$. Differentiating $\mathcal{L}^P$ with respect to p_n^P and equating the resulting expression to zero gives (12). Integrating the terms $\int p_n^P C_n^{P\prime}\mathrm{d}x$ on the interval $[0, L]$ by parts enables to differentiate $\mathcal{L}^P$ with respect to C_n^P and $C_n^P(L)$. Equating the result to zeros gives rise to

$$\begin{cases} \frac{\mathrm{d}p_n^P}{\mathrm{d}x} - p_n^P\alpha(I_n(a))\frac{h(a)}{Q_0} - \frac{h(a)}{VN_z}\gamma(I_n(a)) &= 0 \\ p_n^P(L) - p_n^P(0)P &= 0. \end{cases} \tag{13}$$

Given a vector a, let us still denote by C_n^P, p_n^P the corresponding solutions of (12) and (13). The gradient $\nabla\bar{\mu}_\Delta^P(a)$ is obtained by $\nabla\bar{\mu}_\Delta^P(a) = \partial_a\mathcal{L}^P$, where

$$\begin{aligned}\partial_a\mathcal{L}^P = &\frac{1}{VN_z}\sum_{n=1}^{N_z}\int_0^L \Big(-\gamma'(I_n(a))C_n^P \\ &+\zeta'(I_n(a))\Big)h(a)\partial_a I_n(a)\mathrm{d}x \\ &+\frac{1}{VN_z}\sum_{n=1}^{N_z}\int_0^L \Big(-\gamma(I_n(a))C_n^P + \zeta(I_n(a))\Big)\partial_a h(a)\mathrm{d}x \\ &+\sum_{n=1}^{N_z}\int_0^L p_n^P\Big(-\alpha'(I_n(a))C_n^P + \beta'(I_n(a))\Big)\frac{h(a)}{Q_0}\partial_a I_n(a)\mathrm{d}x \\ &+\sum_{n=1}^{N_z}\int_0^L p_n^P\Big(-\alpha(I_n(a))C_n^P + \beta(I_n(a))\Big)\frac{\partial_a h(a)}{Q_0}\mathrm{d}x.\end{aligned}$$

3.3 Optimization problem for variable reactor volume

In this section, we focus on the case where the reactor volume can also vary. As we have mentioned in Remark 1, we apply an extra assumption to determine X as a function of the volume. Therefore, we apply the parameterization (10) and follow the computations in Bernard et al. (2021b) to determine X. Such parameterization allows us to control the biomass X and the volume of the system V by using an extra parameter a_0. Since both of these two quantities vary with the parameter a_0, maximizing areal productivity is a more relevant target. For a given biomass concentration X, the productivity per unit of surface is defined by:

$$\Pi := \bar{\mu}X\frac{V}{S}, \tag{14}$$

where S presents the ground surface of the raceway pond. From (Bernard et al., 2021a, Appendix C), we have $X = \frac{\alpha_2}{a_0} - \alpha_3$ with $\alpha_2 = \frac{1}{\alpha_0}\ln(\frac{I_s}{I_{\bar{z}_b}})$ and $\alpha_3 = \frac{\alpha_1}{\alpha_0}$, where α_0, α_1 are given in (8).

Consider the extend parameter vector $\tilde{a} := [a_0, a] \in \mathcal{R}^{M+1}$. From (14) and (11), the objective function is given by

$$\Pi_\Delta^P(\tilde{a}) := \frac{\frac{\alpha_2}{a_0} - \alpha_3}{LN_z}\sum_{n=1}^{N_z}\int_0^L \mu(C_n^P, I_n(a))h(a)\mathrm{d}x. \tag{15}$$

The corresponding optimization problem reads:

Find a permutation matrix $P_{\max}$ and a parameter vector $\tilde{a}^*$ solving the maximization problem:

$$\max_{P\in\mathcal{P}}\max_{\tilde{a}\in\mathcal{R}^{M+1}}\Pi_\Delta^P(\tilde{a}).$$

3.4 Optimization procedure for variable reactor volume

Let us denote by $\tilde{\mathcal{L}}^P$ the Lagrangian associated to (15). We follow the same optimization procedure presented in Section 3.2. Note that an extra element appears in this gradient, which is the partial derivative of $\tilde{\mathcal{L}}^P$ with respect to the variable a_0. More precisely, we have $\nabla\Pi_\Delta^P(\tilde{a}) = [\partial_{a_0}\tilde{\mathcal{L}}^P, \partial_a\tilde{\mathcal{L}}^P]$ where

$$\begin{aligned}\partial_{a_0}\tilde{\mathcal{L}}^P = &\frac{\frac{\alpha_2}{a_0} - \alpha_3}{LN_z}\sum_{n=1}^{N_z}\int_0^L \Big(-\gamma'(I_n(\tilde{a}))C_n^P \\ &+\zeta'(I_n(\tilde{a}))\Big)h(\tilde{a})\partial_{a_0}I_n(\tilde{a})\mathrm{d}x \\ &+\frac{\frac{\alpha_2}{a_0} - \alpha_3}{LN_z}\sum_{n=1}^{N_z}\int_0^L \Big(-\gamma'(I_n(\tilde{a}))C_n^P \\ &+\zeta'(I_n(\tilde{a}))\Big)\partial_{a_0}h(\tilde{a})\mathrm{d}x \\ &-\frac{\frac{\alpha_2}{a_0^2}}{LN_z}\sum_{n=1}^{N_z}\int_0^L \Big(-\gamma(I_n(\tilde{a}))C_n^P + \zeta(I_n(\tilde{a}))\Big)h(\tilde{a})\mathrm{d}x \\ &+\sum_{n=1}^{N_z}\int_0^L p_n^P\Big(-\alpha'(I_n(\tilde{a}))C_n^P \\ &+\beta'(I_n(\tilde{a}))\Big)\frac{h(\tilde{a})}{Q_0}\partial_{a_0}I_n(\tilde{a})\mathrm{d}x \\ &+\sum_{n=1}^{N_z}\int_0^L p_n^P\Big(-\alpha(I_n(\tilde{a}))C_n^P + \beta(I_n(\tilde{a}))\Big)\frac{\partial_{a_0}h(\tilde{a})}{Q_0}\mathrm{d}x,\end{aligned}$$

and $\partial_a\tilde{\mathcal{L}}^P$ is similar to $\partial_a\mathcal{L}^P$.

4. NUMERICAL RESULTS

In this section, we present some numerical results derived from the optimization procedure presented in the previous section. Note that for a given vertical discretization number N_z, we need to test all the permutation matrices in the set $\mathcal{P}$, which means $N_z!$ possible cases. Since an optimization problem must be solved for each permutation matrix the problem is highly computational demanding and we consider in the following tests $N_z = 7$ for which the problem is solvable in reasonable time. Note also that for the Fourier truncated number, the larger M, the less valid is our hydrodynamic model, see Section 2.1, where a smooth topography is assumed to guarantee a laminar regime. Hence, limit situations where $M \to +\infty$ are not considered and $M = 5$ in what follows. Regarding the parameterization of h, we use truncated Fourier series presented in (10).

4.1 Numerical solver

We introduce a supplementary space discretization with respect to x to solve numerically our optimization problem. Let us take a space discretization number N_x, set $\Delta x = L/N_x$ and $x^{n_x} = n_x\Delta x$ for $n_x = 0, \ldots, N_x$. We choose to apply the Heun's scheme to compute C_n^P via (12). Following a first-discretize-then-optimize strategy, we get that the Lagrange multiplier p_n^P is also computed by a Heun's type scheme via (13). We use the Gradient-based algorithm to solve the optimization problem with the subcritical constraint.

4.2 Parameter for the models

The spatial discretization number is set to $N_x = 1001$ points such that the convergence of the numerical scheme has been ensured, and we take the averaged discharge $Q_0 = 0.04\,\mathrm{m}^2 \cdot \mathrm{s}^{-1}$, and $z_b(0) = -0.4\,\mathrm{m}$ to stay in standard ranges for a raceway pond. The free-fall acceleration is set to be $g = 9.81\,\mathrm{m} \cdot \mathrm{s}^{-2}$. All the numerical parameters values for Han's model are taken from Grenier et al. (2020). For fixed volume, we assume that only 1% of light can be captured by the cells at the bottom of the raceway, under our parameterization, the light extinction coefficient ε can be computed by $\varepsilon = (1/a_0)\ln(1/1\%)$. For varying volume, the specific light extinction coefficient of the microalgae specie $\alpha_0 = 0.2\,\mathrm{m}^2 \cdot \mathrm{gC}$ and the background turbidity coefficient $\alpha_1 = 10\,\mathrm{m}^{-1}$, these are taken from Martínez et al. (2018). Besides, $I_s = 2000\,\mu\mathrm{mol} \cdot \mathrm{m}^{-2}\,\mathrm{s}^{-1}$ which corresponds to the order of magnitude of the maximum light intensity in summer in the south of France.

4.3 Numerical tests

We present some results for both constant and non constant volume. We will show the optimal permutation matrices and the associated shape of the topographies for these two frameworks and compare the gain with a standard system.

Constant volume The first test is dedicated to study the optimal permutation matrix and the associated shape of the topography for constant volume. To evaluate the efficiency of the corresponding mixing strategy, define:

$$r_1 := \frac{\bar{\mu}_\Delta^{P_{\max}}(a^*) - \bar{\mu}_\Delta^{P_{\max}}(0)}{\bar{\mu}_\Delta^{P_{\max}}(0)}, r_2 := \frac{\bar{\mu}_\Delta^{P_{\max}}(a^*) - \bar{\mu}_\Delta^{\mathcal{I}_{N_z}}(0)}{\bar{\mu}_\Delta^{\mathcal{I}_{N_z}}(0)}. \tag{16}$$

Here r_1 defines the gain of the optimal permutation strategy with the optimal topography compare to the optimal permutation strategy with a flat topography, and r_2 defines the gain of the optimal permutation strategy with the optimal topography compare to no permutation strategy with a flat topography. We fix the volume related parameter $a_0 (= h(0;a)) = 0.4\,\mathrm{m}$ to stay in a standard raceway pond range. The initial guess of the vector a is set to be 0, which corresponds to a flat topography. Let us consider two raceway pond length $L = 100\,\mathrm{m}$ and $L = 1\,\mathrm{m}$ respectively. The optimal matrices $P_{\max}$ for different L are denoted by $P_{\max}^L$ and given in (17) with the associated optimal topographies presented in Fig. 2. A non flat topography associated with a non trivial permutation matrix has been observed. In particular, these optimal matrices corresponds to the optimal matrices obtained with a flat topography under the same parameter settings (Bernard et al., 2021b, Equation 11,Equation 13). The two ratios defined in (16) are $r_1 = 0.148\%$, $r_2 = 1.070\%$ and $r_1 = 0.001\%$ $r_2 = 3.453\%$ respectively.

$$P_{\max}^{100} = \begin{pmatrix} 0&1&0&0&0&0&0\\ 0&0&0&1&0&0&0\\ 0&0&0&0&0&1&0\\ 0&0&0&0&0&0&1\\ 0&0&0&0&1&0&0\\ 0&0&1&0&0&0&0\\ 1&0&0&0&0&0&0 \end{pmatrix}, \; P_{\max}^{1} = \begin{pmatrix} 1&0&0&0&0&0&0\\ 0&0&0&0&0&0&1\\ 0&0&0&0&0&1&0\\ 0&0&0&0&1&0&0\\ 0&0&0&1&0&0&0\\ 0&0&1&0&0&0&0\\ 0&1&0&0&0&0&0 \end{pmatrix} \tag{17}$$

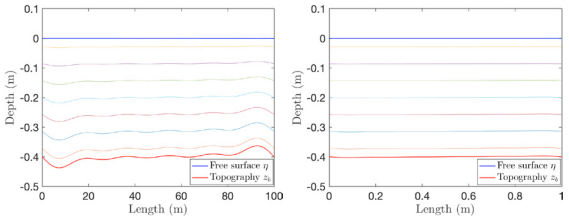

Fig. 2. The optimal topographies and the associated trajectories for the permutation matrices (17). Left: $L = 100\,\mathrm{m}$. Right: $L = 1\,\mathrm{m}$.

As we observed in the test above, the length of raceway has a potential influence on the objective function and the gain, we then provide a test for different values of the length L. Fig. (3) shows the objective function $\bar{\mu}_\Delta$ and the two ratios r_1, r_2 as a function of the length L. Note that the objective function decreases when L increases except in the neighbourhood of $L = 12.5\,\mathrm{m}$, on the same time, we observe that the influence of topography is very limited comparing to the influence of the permutation strategies.

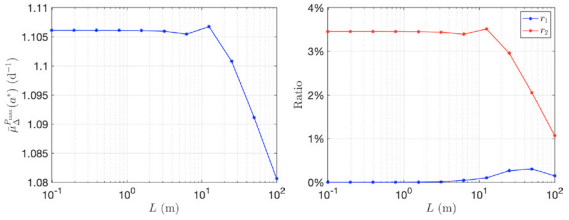

Fig. 3. The optimal value of the objective function $\bar{\mu}_\Delta$ (top) and the two ratios r_1, r_2 (bottom) for $L = 100/2^{\{0,\dots,10\}}$.

Varying volume We consider now that the volume can vary. Note that the volume related coefficient a_0 is also a parameter to be optimized. Let us define two ratios similar as (16) to evaluate the efficiency of the permutation strategies,

$$\begin{aligned} \tilde{r}_1 &:= \frac{\Pi_\Delta^{P_{\max}}(\tilde{a}^*) - \Pi_\Delta^{P_{\max}}(\tilde{a}_f)}{\Pi_\Delta^{P_{\max}}(\tilde{a}_f)}, \\ \tilde{r}_2 &:= \frac{\Pi_\Delta^{P_{\max}}(\tilde{a}^*) - \Pi_\Delta^{\mathcal{I}_{N_z}}(\tilde{a}_f)}{\Pi_\Delta^{\mathcal{I}_{N_z}}(\tilde{a}_f)}, \end{aligned} \tag{18}$$

where $\tilde{a}_f := [\tilde{a}_0^*, 0, \cdots, 0]$ and $\tilde{a}_0^*$ is the optimal volume related value. The initial guess of $\tilde{a}$ is set to be a null vector except $\tilde{a}_0^* = 0.4$ as initial value. We keep the same length setting as in constant volume test, the optimal matrices $P_{\max}^L$ are given in (19) and the associated optimal topographies are presented in Fig. 4. The two ratios defined in (18) are $\tilde{r}_1 = 0.918\%$, $\tilde{r}_2 = 9.284\%$ and $\tilde{r}_1 = 0.00003\%$, $\tilde{r}_2 = 12.714\%$ respectively.

$$P_{\max}^{100} = \begin{pmatrix} 0&0&0&1&0&0&0\\ 0&0&0&0&0&1&0\\ 0&0&0&0&0&0&1\\ 0&0&0&0&1&0&0\\ 0&0&1&0&0&0&0\\ 0&1&0&0&0&0&0\\ 1&0&0&0&0&0&0 \end{pmatrix}, \; P_{\max}^{1} = \begin{pmatrix} 0&0&0&0&0&0&1\\ 0&0&0&0&0&1&0\\ 0&0&0&0&1&0&0\\ 0&0&0&1&0&0&0\\ 0&0&1&0&0&0&0\\ 0&1&0&0&0&0&0\\ 1&0&0&0&0&0&0 \end{pmatrix} \tag{19}$$

As shown experimentally in the previous test, the influence of the topographies remain limited, at the same time,

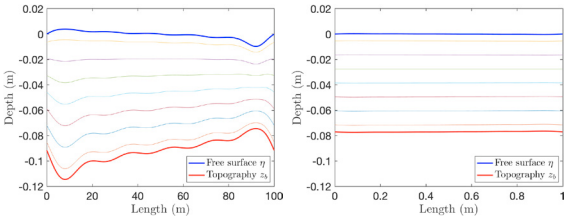

Fig. 4. The optimal topographies and the associated trajectories for the permutation matrices (19). Left: $L = 100\,\mathrm{m}$. Right: $L = 1\,\mathrm{m}$.

non trivial permutation strategies $P^L_{\max}$ are obtained for different raceway length L, in particular these strategies are also different from the case with a fixed volume. Moreover, these strategies have a better improvement when the volume is also optimized. Note that in this case the algorithm stops before finding an optimum since it is limited by the constraint subcritical flow. Fig. 5 shows the objective function Π_Δ and the two ratios $\tilde{r}_1, \tilde{r}_2$ as a function of the length L. Note that the average growth rate Π_Δ increase when L goes to 0. This *flashing effect* corresponds to the fact that the algae exposed to high frequency flashing have a better growth. This phenomenon has already been reported in literature (e.g. Bernard et al., 2021b; Lamare et al., 2019).

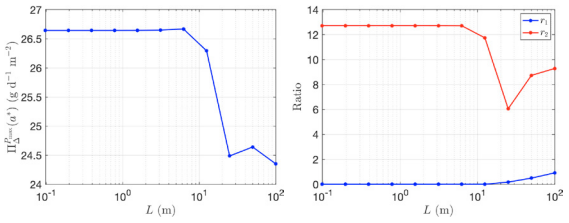

Fig. 5. The optimal value of the objective function Π_Δ (top) and the two ratios $\tilde{r}_1, \tilde{r}_2$ (bottom) for $L = 100/2^{\{0,\dots,10\}}$.

5. CONCLUSION

Adapting the shape of the raceway to an original mixing system is an innovative strategy to boost the algal process productivity. To realize in practice the ideal mixing a system more elaborated than a paddle wheel is required.

However, with the Han parameter considered for this species the gain stays limited and would not compensate a higher cost due to the more complicate design of the bottom topography and of the mixing device. It is possible that a higher gain is also obtained when leaving the laminar regime, but the energy dissipation in a turbulent regime would lead to a strong enhancement of the operating costs.

ACKNOWLEDGEMENTS

This research benefited from the support of the FMJH ProgramPGMO and from the support to this program from EDF-THALES-ORANGE

REFERENCES

Bernard, O., Lu, L.D., Sainte-Marie, J., and Salomon, J. (2021a). Shape optimization of a microalgal raceway to enhance productivity. URL (Preprint) https://hal.archives-ouvertes.fr/hal-02994713. Submitted paper.

Bernard, O., Lu, L.D., and Salomon, J. (2021b). Optimizing microalgal productivity in raceway ponds through a controlled mixing device. URL (Preprint) https://hal.archives-ouvertes.fr/hal-02970756. To appear in the Proceedings of the 2021 American Control Conference (ACC 2021).

Chiaramonti, D., Prussi, M., Casini, D., Tredici, M.R., Rodolfi, L., Bassi, N., Zittelli, G.C., and Bondioli, P. (2013). Review of energy balance in raceway ponds for microalgae cultivation: Re-thinking a traditional system is possible. *Applied Energy*, 102, 101–111.

Chisti, Y. (2007). Biodiesel from microalgae. *Biotechnology Advances*, 25(3), 294 – 306.

Demory, D., Combe, C., Hartmann, P., Talec, A., Pruvost, E., Hamouda, R., Souillé, F., Lamare, P.O., Bristeau, M.O., Sainte-Marie, J., Rabouille, S., Mairet, F., Sciandra, A., and Bernard, O. (2018). How do microalgae perceive light in a high-rate pond? towards more realistic lagrangian experiments. *The Royal Society*.

Gerbeau, J.F. and Perthame., B. (2001). Derivation of viscous saint-venant system for laminar shallow water; numerical validation. *Discrete & Continuous Dynamical Systems - B*, 1(1), 89–102.

Grenier, J., Lopes, F., Bonnefond, H., and Bernard, O. (2020). Worldwide perspectives of rotating algal biofilm up-scaling. Submitted paper.

Grognard, F., Akhmetzhanov, A.R., and Bernard, O. (2014). Optimal strategies for biomass productivity maximization in a photobioreactor using natural light. *Automatica*, 50(2), 359–368.

Han., B.P. (2001). Photosynthesis–irradiance response at physiological level: A mechanistic model. *Journal of theoretical biology*, 213(2), 121–127.

Lamare, P.O., Aguillon, N., Sainte-Marie, J., Grenier, J., Bonnefond, H., and Bernard, O. (2019). Gradient-based optimization of a rotating algal biofilm process. *Automatica*, 80–88.

Martínez, C., Mairet, F., and Bernard, O. (2018). Theory of turbid microalgae cultures. *Journal of Theoretical Biology*, 456, 190–200.

Masci, P., Grognard, F., and Bernard, O. (2010). Microalgal biomass surface productivity optimization based on a photobioreactor model. *IFAC Proceedings Volumes*, 43(6), 180–185.

Perner, I., Posten, C., and Broneske, J. (2003). Cfd optimization of a plate photobioreactor used for cultivation of microalgae. *Engineering in Life Sciences*, 3(7), 287–291.

Wijffels, R.H. and Barbosa, M.J. (2010). An outlook on microalgal biofuels. *Science*, 329(5993), 796–799.